The Astronomical Journal, 166:91 (10pp), 2023 September https://doi.org/10.3847/1538-3881/ace782

Age Distribution of Exoplanet Host Stars: Chemical and Kinematic Age Proxies from GAIA DR3

C. Swastik[1,2], Ravinder K. Banyal[1], Mayank Narang[3], Athira Unni[5], Bihan Banerjee[4], P. Manoj[4], and T. Sivarani[1]
[1] Indian Institute of Astrophysics, Koramangala 2nd Block, Bangalore 560034, India; swastik.chowbay@iiap.res.in
[2] Pondicherry University, R.V. Nagar, Kalapet, 605014, Puducherry, India
[3] Academia Sinica Institute of Astronomy & Astrophysics, 11F of Astro-Math Building, No. 1, Section 4, Roosevelt Road, Taipei 10617, Taiwan, Republic of China
[4] Department of Astronomy and Astrophysics, Tata Institute of Fundamental Research Homi Bhabha Road, Colaba, Mumbai 400005, India
[5] Aryabhatta Research Institute of Observational Sciences, Manora Peak, Nainital 263002, Uttarakhand, India
Received 2023 February 16; revised 2023 June 28; accepted 2023 July 9; published 2023 August 4

Abstract

The GAIA space mission is impacting astronomy in many significant ways by providing a uniform, homogeneous, and precise data set for over 1 billion stars and other celestial objects in the Milky Way and beyond. Exoplanet science has greatly benefited from the unprecedented accuracy of the stellar parameters obtained from GAIA. In this study, we combine photometric, astrometric, and spectroscopic data from the most recent Gaia DR3 to examine the kinematic and chemical age proxies for a large sample of 2611 exoplanets hosting stars whose parameters have been determined uniformly. Using spectroscopic data from the Radial Velocity Spectrometer on board GAIA, we show that stars hosting massive planets are metal-rich and α-poor in comparison to stars hosting small planets. The kinematic analysis of the sample reveals that stellar systems with small planets and those with giant planets differ in key aspects of galactic space velocity and orbital parameters, which are indicative of age. We find that the galactic orbital parameters have a statistically significant difference of 0.06 kpc for $Z_{\max}$ and 0.03 for eccentricity, respectively. Furthermore, we estimated the stellar ages of the sample using the MIST-MESA isochrone models. The ages and their proxies for the planet-hosting stars indicate that the hosts of giant planetary systems are younger when compared to the population of stars harboring small planets. These age trends are also consistent with the chemical evolution of the galaxy and the formation of giant planets from the core-accretion process.

Unified Astronomy Thesaurus concepts: Planet formation (1241); Exoplanet formation (492); Gaia (2360); Extrasolar gaseous giant planets (509); Stellar kinematics (1608); Stellar ages (1581); Metallicity (1031); Chemical abundances (224); Exoplanets (498); Spectroscopy (1558)

1. Introduction

Unprecedented advances in astronomy and astrophysics are being achieved through the GAIA space mission. This is made possible by the sheer volume and quality of the data obtained from the high-precision spectroscopic, astrometric, and photometric instruments on board GAIA (Gaia Collaboration et al. 2018, 2022). GAIA's impact on exoplanet science is no less impressive. The planet discovery potential of the GAIA mission was first investigated by Perryman et al. (2014). Astrometry is an important detection technique that can provide both the mass and orbital period of the planet. In the next data release, GAIA is expected to detect several thousand new exoplanets thanks to its 30-fold increase in astrometric precision when compared to its predecessor, HIPPARCOS (van Leeuwen 1997). However, GAIA's contribution to exoplanet science goes beyond detecting planets by astrometry.

GAIA has enabled stellar and planetary radii to be derived with the highest possible accuracy (∼5%) using the most precise parallaxes to date (Berger et al. 2018, 2020a). Accurate stellar and planetary radii have thus helped to solidify star-planet correlations, such as planet-radius versus stellar metallicity (Buchhave et al. 2014; Narang et al. 2018; Schlaufman 2018). Furthermore, the existence of the "radius valley," which is a gap in the distribution of exoplanet radii that separates the super-Earths ($R \sim 1.4R_{\oplus}$) and mini-Neptunes ($R \sim 2.4R_{\oplus}$), with a clear paucity around $R \sim 1.8R_{\oplus}$, is now well established from observational results (Fulton et al. 2017; Armstrong et al. 2019; Petigura et al. 2022).

Significant research effort has also been devoted to exploring star-planet connections, showing how the fundamental properties of stars determine the orbital and physical characteristics of the planetary systems. For example, spectroscopic studies have shown that the metallicity distribution of stars with small ($M_P < 0.3M_J$) and giant planets ($0.3M_J \leqslant M_P \leqslant 13M_J$) is different, indicating that they likely belong to different populations and also that metallicity plays a key role in giant planet formation (Gonzalez 1997; Santos et al. 2001; Fischer & Valenti 2005; Udry & Santos 2007; Buchhave et al. 2012, 2014; Dong et al. 2014; Fleming et al. 2015; Johnson et al. 2017; Mulders 2018; Narang et al. 2018; Petigura et al. 2018; Swastik et al. 2021). Furthermore, a detailed abundance analysis shows that the chemical composition of stars hosting small and giant planets is different, with the latter being α-poor (Swastik et al. 2022; Unni et al. 2022). Using [α/Fe] ratio as a proxy for the age, these studies suggest that the small planetary systems may have started forming early in the Milky Way's history when compared to the late formation onset of the giant planets (Delgado Mena et al. 2019). Estimating the ages from isochrone fittings for a subsample of exoplanet-hosting stars have also arrived at similar conclusions (Bonfanti et al. 2015; Swastik et al. 2022). these age differences are also reported

based on the position and kinematic studies of the confirmed population of planet-hosting stars (Narang et al. 2023 under review).

Important as they are, the majority of these studies used mixed samples of stars that were originally observed in different planet search and follow-up surveys (Santos et al. 2011; Brewer et al. 2016; Brewer & Fischer 2018). In most cases, the stellar properties themselves are determined using different observing strategies, instrument settings, and analysis methods. This results in various systemics and offsets, making the interpretation and comparison more difficult across different studies. Ideally, to make the findings more robust and universal, a sufficiently large sample of stars should be observed with the same equipment under similar conditions and a uniform methodology must be applied to determine the parameters of interest. With the latest release of the GAIA DR3 data, it is possible to study a much larger and uniform sample of planet-hosting stars whose properties have been determined homogeneously.

The General Stellar Parametriser (GSP) module uses spectra from a medium-resolution (R $\sim$11,500) radial velocity spectrograph (Recio-Blanco et al. 2023). The GSP-Spec module computes the stellar atmospheric parameters ($T_{\rm eff}$, log$g$, metallicity ([M/H])) and abundances ([X/Fe]) for 13 species for each star, including three Fe-peak elements, Cr, Ni, and Fe. Additionally, it provides the mean abundances of eight α-elements (O, Ne, Mg, Si, S, Ar, Ca, and Ti) in the catalog. Other than spectroscopic parameters, GAIA also provides homogeneous and accurate astrometric and photometric parameters for nearly two billion stars, which is the largest to date.

In this paper, we investigate a sample of 2611 planet-hosting stars whose parameters have been determined homogeneously. We used the Gaia DR3 data, and analyzed the spectroscopic and kinematic parameters of stars hosting small and giant planets. The outline of this paper is as follows. We describe our sample in Section 2. We report the results of the spectroscopic, kinematic, and isochrone age analyzes in Section 3. In Section 4, we briefly discuss our results in the context of planet formation theories, and also elude to possible biases and systematic affecting our findings. Finally, in Section 5, we conclude and summarize the results.

2. The Sample

For this study, we used the confirmed list of exoplanetary systems from the NASA exoplanet archive (Akeson et al. 2013; NASA Exoplanet Science Institute 2020) and cross-matched it with the latest Gaia data release DR3 to obtain the stellar data for the planet-hosting stars. We first employed the Astronomical Data Query Language (ADQL) to identify the GAIA DR3 source IDs associated with our exoplanet-hosting stars. Subsequently, we utilized ADQL to extract the corresponding data from the Astrophysical parameters table. In cases where multiple matches were found, we manually verified the G-Band magnitude quoted in the NASA exoplanet archive and selected the closest match to the search result in the GAIA DR3 data set. Additionally, for the purpose of validation, we used TOPCAT to perform R.A.-decl. cross-matching with a search radius[6] of 3″ and obtained identical results to those extracted using ADQL.

In the case of GAIA, the spectroscopic data is obtained from the Radial Velocity Spectrometer (RVS) instrument on board GAIA, which is a medium-resolution spectrograph. The data products from the RVS spectra are listed in the Astrophysical parameters table. Furthermore, each parameter is associated with a quality flag[7] indicating the quality of the data. For the analysis presented in this paper, most of our samples are associated with the best-quality flag (zero in this case) and we excluded the stars with low-quality data flags (nine in this case). Therefore, our primary sample consists of 2611 planet-hosting stars (accounting for 3553 planetary companions) for which the radial velocity data was available from the GAIA archive. The sample extracted from GAIA and the important parameters derived in this paper are listed in Table 1. Figure 1 shows the distribution of these stars in Mollweide projection, while Figure 2 shows the distribution of planet mass whose sources are listed in the GAIA archive.

Since the original sample contained many evolved stars, notably giants and subgiants, we restricted our analysis to the main-sequence stars because it is difficult to account for the NLTE and other evolutionary effects that can alter the surface abundances of the evolved stars (Swastik et al. 2022). We followed the procedure of Brewer & Fischer (2018) to exclude the evolved stars using $T_{\rm eff}$ and log g cutoff. Furthermore, we included only those host stars where the companion mass $<13M_J$. In addition, to avoid bias from possible mixing, we also excluded stars with multi-planetary systems containing a combination of small and giant planets. After applying these filters, our final sample was trimmed to 971 stars with 1309 planets for which the spectroscopy data is available and 2130 stars with 2861 planets for which astrometric data is available. After estimating the stellar ages (more details are given in Section 3.3), we included only those stars whose uncertainties are $<$ their main-sequence lifetime, as suggested by Pont & Eyer (2004). We also excluded the lower main-sequence stars from our age sample ($T_{\rm eff} < 4400$ K) because the isochrone ages for the lower main-sequence stars are not very accurate given the large uncertainties. Thus, after curation, we analyzed the ages of 806 stars hosting 1071 planets. In this sample, about $\sim$83% of stars in the astrometrically curated sample belong to transit surveys (mostly Kepler) and $\sim$17% belong to different RV surveys. In the spectroscopic sample, $\sim$64% stars are from transit discoveries, while the remaining stars come from the RV detections. Additionally, the spectroscopic sample is a subset of the astrometric sample, which means that the astrometric data is available for all stars belonging to the spectroscopic sample.

3. Results

We used different proxies of stellar ages from spectroscopic, photometric, and astrometric data from the GAIA DR3 to analyze the confirmed exoplanet population. In this section, we present the results that we obtained from the GAIA DR3 data in the context of planet formation.

3.1. Spectroscopic Analysis of the Planet Hosts Stars

Gaia DR3 provides a significantly large sample of stars whose spectroscopic parameters are determined homogeneously. The

[6] Initially, we used a larger search radius and found that most of the planet-hosting stars can be extracted with a search radius of 3″. For cases where we were not able to obtain the matches, we increased the search radius up to 15″ and also checked for the G-band magnitude to confirm if the target is indeed a planet-hosting star.

[7] For more details on the quality flag, see Table 2 of Recio-Blanco et al. (2023).

Table 1
Key Parameters of Exoplanet-hosting Stars used or Estimated in This Study

TIC ID	hostname	Method	Planet	Pl- Mass(M_J)	R.A.	Decl.	Parallax (mas)
TIC 328465904	CD Cet	Radial Velocity	CD Cet b	0.01243	48.3530155	4.7751881	116.267814433972
TIC 380966347	HD 14787	Radial Velocity	HD 14787 b	1.121	35.8085099	10.8367972	8.45391699045641
TIC 435339847	K2-77	Transit	K2-77 b	1.9	55.228521	12.572448	7.08178354133806
TIC 435339558	K2-79	Transit	K2-79 b	0.0415	55.2559307	13.5191871	3.8412449465656
TIC 242961495	K2-80	Transit	K2-80 b	0.0148	59.037486	13.5590288	5.02001944435433
TIC 242961495	K2-80	Transit	K2-80 c	0.00869	59.037486	13.5590288	5.02001944435433
...							

Note. The entire table is available in machine-readable format. For simplicity, only the first six rows and eight columns are shown here.

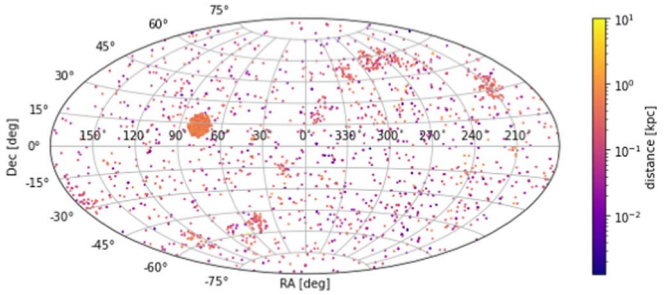

Figure 1. Exoplanet-hosting stars for which Gaia parameters are available. The color bar represents the distance in kpc from the Sun. In addition, note the blob of the planet above the galactic plane that represents the Kepler field.

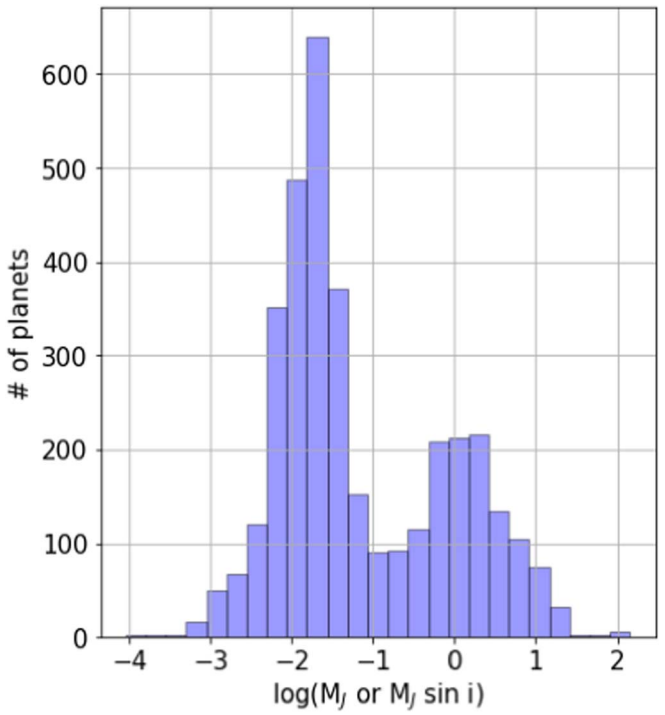

Figure 2. Planet-mass distribution for the sample with host stars listed in the GAIA archive.

GSP-Spec module (Recio-Blanco et al. 2023) does the spectroscopic processing using the combined RVS spectra of single stars to calculate stellar chemo-physical characteristics. The RVS covers a spectral range of 846–870 nm and has a resolution of $R \sim 11{,}500$ (Cropper et al. 2018). The GSP-Spec module estimates the stellar atmospheric parameters ($T_{\rm eff}$, $\log g$, [M/H][8]) and the abundances of 13 chemical species (N, Mg, Si, S, Ca, Ti, Cr, Fe I, Fe II, Ni, Zr, Ce, and Nd). The stellar atmospheric parameters are estimated using the Matisse GAUGUIN algorithm and artificial neural network (ANN; Recio-Blanco et al. 2016, 2023). However, the abundances are obtained solely from the Matisse GAUGUIN algorithm using Gaussian fitting methods (Zhao et al. 2021; Recio-Blanco et al. 2023). For the analysis presented in this paper, we used the stellar parameters and abundances from the Matisse GAUGUIN algorithm.

Since GAIA spectroscopic data from the GSP-Spec module suffers from estimation biases (Recio-Blanco et al. 2023), we used the HARPS-GTO sample (a high-resolution sample of 1111 stars targeted mainly with the goal of detecting planets by radial velocity) for calibration (Mayor et al. 2003; Lo Curto et al. 2010; Santos et al. 2011). After taking care of the calibration and possible estimation biases, as discussed in Appendix, we investigated the host star metallicities and [Mg/Fe] (a proxy for overall α abundances) in the GAIA archive as a function of planet mass. We chose [Mg/Fe] because we wanted to investigate the ratio of the abundances of elements produced from Type II supernovae (Mg) to Type I supernovae (Fe). In addition, since the major production site for Mg is Type II supernovae, it is the strongest tracer for the overall α abundance in a star (Kobayashi et al. 2020). We used the planet mass from the NASA exoplanet archive (Akeson et al. 2013; NASA Exoplanet Science Institute 2020)[9] and binned the data appropriately in terms of planet mass depending on the number of stars in each bin, with four bins for small planet-hosting stars ($M_P < 0.3M_J$), two for giants ($0.3M_J \leqslant M_P \leqslant 4M_J$), and one for super-Jupiters ($M_P > 4\ M_J$). We found that the host star metallicity increases as a function of planet mass with a turn-around after $\sim$4 M_J, as seen in Figure 3. Although several studies have shown similar results (Fischer & Valenti 2005; Valenti & Fischer 2008; Narang et al. 2018; Swastik et al. 2021), they were mostly limited to either small samples or inhomogeneous measurements of metallicities. In this paper, we were able to reproduce these results for a large number of exoplanet-hosting stars using the data from the RVS spectra from the GAIA DR3.

We also find that there is a decreasing trend with planet mass for the α-element abundances ([Mg/Fe]), as seen in Figure 3. For comparison with α element, we used only Fe abundances because abundances of only two other Fe-peak elements (Ni and Cr) were available, and Fe is estimated with

[8] Here [M/H] is defined as the total metal content of the star.

[9] For the planets detected by transits, we used the planet mass–radius relationship from (Chen & Kipping 2017). For the planets detected by RV, we used the minimum mass (M.sin$i$) as listed in the NASA exoplanet archive.

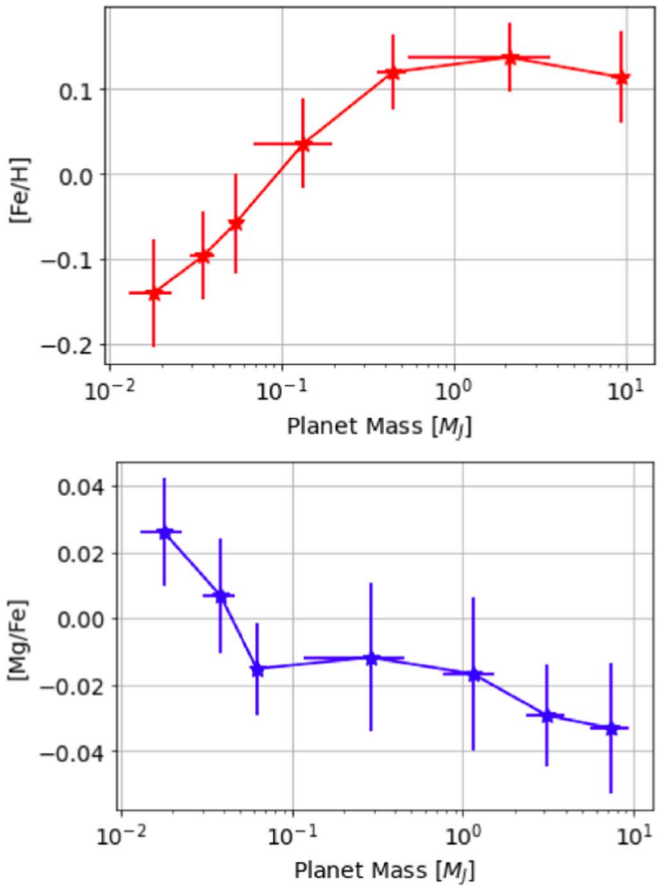

Figure 3. Top panel: Host star metallicity as a function of planet mass. Bottom panel: [Mg/Fe] of planet-hosting stars as a function of planet mass. The errors in metallicity and Mg abundances are represented by the standard error of the mean, whereas the errors in planet mass are represented by the standard deviation in each bin.

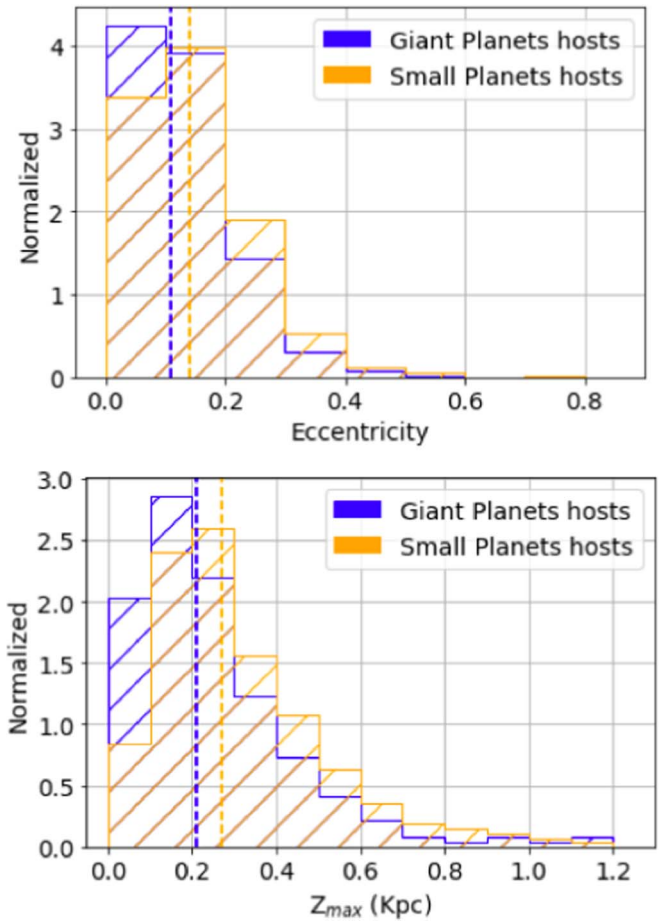

Figure 4. Galactic orbital parameters for the small and giant planet-hosting stars. Top panel: Eccentricity distribution for the planet-hosting stars (binned at 0.1 dex). Bottom panel: Z_{max} distribution for the different populations of exoplanet-hosting stars (binned at 0.1 Kpc). The vertical lines represent the median of the distribution for the small and giant planet hosts.

much better precision compared to Ni and Cr in the GAIA GSP-Spec module. Since [Fe/H] and α-enhancement are proxies for the ages of a population of stars (Delgado Mena et al. 2019; Swastik et al. 2022), the decline in α-abundances together with enhancement of [Fe/H] indicate that giant planets are preferentially hosted by younger stars, while the stars having small planetary companions have a wider spread in the age.

3.2. Kinematic Analysis of Exoplanet-hosting Stars

The kinematic analysis of stars entails tracking the past motions of a group of stars to determine when they were physically closest, which is thought to be the period of their formation. In this case, stellar parameter estimation, such as the galactic space velocities (*U, V,* and *W*) and orbital parameters (eccentricity and Z_{max}), is based on minimal assumptions and does not need stellar modeling but high-quality astrometry and radial velocities measurements. In our case, we used the radial velocity and proper motion data from the GAIA DR3 data to compute the galactic space velocities (Johnson & Soderblom 1987; Ujjwal et al. 2020). We used galpy (Bovy 2015) to compute the stellar orbital parameters (eccentricity and Z_{max}) and used the solar motion $(U_\odot, V_\odot, W_\odot) = (11.1, 12.24, 7.25)$ km s^{-1} from Schönrich et al. (2010) as a reference. We analyzed a sample of 2130 stars and found that the stars hosting small planets have higher median eccentricity and Z_{max}[10] when compared to giant planet-hosting stars, as can be seen clearly in Figure 4.

Peculiar velocity (ν_{pec})[11] and total velocity dispersion (σ_{tot})[12] distribution have notable differences for small and giant planet-hosting stars, as shown by the red and blue circles in Figure 5. We find that the scatter in the ν_{pec} is much more significant for small planet hosts than for giant planet-hosting stars. For example, in the case of small planet hosts, 50% and 80% of the population lies at a velocity radius of 46 and 69 km s^{-1}, compared to 38 and 60 km s^{-1} for giant planet hosts. The age for an ensemble of stars increases radially from the origin, with the thin disk (younger population) stars having low ν_{pec}, and extending to thick disk and halo stars (older population) having higher ν_{pec} (Reddy et al. 2006; Casagrande et al. 2011). The clustering of the giant planet hosts around the origin of the Toomre diagram (Figure 5) indicates that they belong to a statistically younger population of stars when compared to stars hosting small planets, which show a larger spread in ν_{pec} (and

[10] Z_{max} is integral of motion that tells us the maximum height above or below the galactic plane on the disk that a star travels.
[11] $\nu^2_{pec} = U^2_{LSR} + V^2_{LSR} + W^2_{LSR}$; which is represented by the radius drawn from the origin in the Toomre diagram.
[12] $\sigma^2_{tot} = \sigma^2_U + \sigma^2_V + \sigma^2_W$

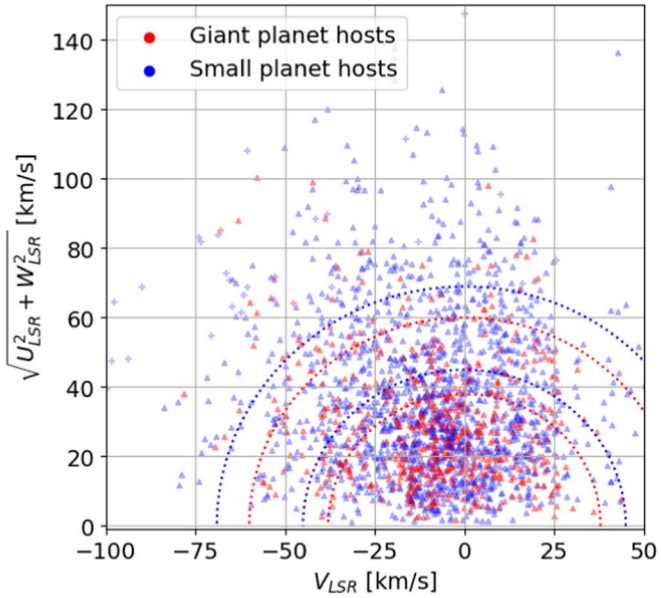

Figure 5. Toomre diagram for the current sample of planet-hosting stars. The blue and red circles represent the locus of ν_{pec} for the small and giant planet hosts. The area enclosed by inner circles has ∼50% of stars population, while the outer circles capture ∼80% of the population in each category.

σ_{tot}). Considering the uncertainties associated with Gaia's proper motion, RV (radial velocity), and parallaxes, we conducted an additional assessment to investigate the impact of these uncertainties on the estimation of ν_{pec} and σ_{tot}. To account for uncertainties in the space motion of stars, we calculated the error in *U, V*, and *W* using the relationships described in Equation (2) of Johnson & Soderblom (1987). The median uncertainties in *U, V*, and *W* were found to be 0.16, 0.49, and 0.17 km s^{-1}, respectively. To determine if these uncertainties affect the analysis presented in this paper, we performed a Monte Carlo simulation where each space velocity component *U, V*, and *W* of a star is randomly generated from a Gaussian distribution with the mean and standard deviation obtained as described above. We then calculated ν_{pec} using these random realizations of *U, V*, and *W* for both small and giant planet-hosting stars. This process was repeated 100,000 times and we find that the 1σ spread in ν_{pec} for small and giant planet hosts is 0.35 and 0.18 km s^{-1}, which is relatively small (Figure 6, top row) compared to the absolute difference in the ν_{pec} between small and giant planets (∼10 km s^{-1}). This suggests that the uncertainties in the Gaia astrometric parameters do not significantly affect the analysis presented in this paper. We also conducted a similar analysis for σ_{tot}, as shown in the bottom row of Figure 6. We have also noted the median and spread obtained from the Monte Carlo analysis for ν_{pec} and σ_{tot} in Table 3.

We classified the likelihood of each star belonging to the thin disk, thick disk, or halo using the approach adopted by Reddy et al. (2006). Therein, the parent sample is considered to be a mixture of the three populations, and it is assumed that every population has a Gaussian random distribution of velocities for each component (Reddy et al. 2006; Adibekyan et al. 2011). By assigning a probability threshold of 70% for a star to belong to a particular population, we find that ∼98% of the planet-hosting stars belong to a thin disk population (Table 2). We also find that the sample of stars hosting small and giant planets cannot be manifested in terms of thin versus thick disk population. In terms of galactic orbital parameters, we find that, on average, stars hosting small planets have higher median eccentricity and Z_{max} compared to giant planet-hosting stars. We also performed an Anderson–Darling (AD) test, and found that the difference is significant for both galactic space velocities and orbital parameters (Table 2), suggesting that small and giant planet-hosting stars likely belong to different populations.

Several studies (e.g., Chen 2003; Casagrande et al. 2011; Wojno et al. 2018; Ness et al. 2019; Bashi & Zucker 2022) have indicated that the higher values of Z_{max}, eccentricity and σ_{tot} are proxies for older stars. For instance, Wojno et al. (2018) found that eccentricity differs by ∼0.05 and z_{max} by ∼ 0.04 for the young ($\leqslant$3 Gyr) and the old ($\geqslant$8 Gyr) stars. For exoplanet-hosting stars, using a limited sample (135 stars) of Neptune, super-Earth, and Jupiter hosts, Adibekyan et al. (2012) have also shown that Jupiter hosting stars have lower median eccentricities and Z_{max} compared to stars hosting Neptunes (see Table 3 of Adibekyan et al. 2012). In our study, this is validated for a larger sample of exoplanet-hosting stars using the astrometric and radial velocity data from GAIA. We note that the distribution of Z_{max}, eccentricity, ν_{pec}, and σ_{tot} are statistically different for stars hosting small and giant planets. For comparison, these parameters along with the *p*-value are listed in Table 2.

3.3. Ages of Planet-hosting Stars

Yet another way to distinguish the parent stars of small and giant planets is to directly estimate their ages. Asteroseismology is the only technique that can determine a star's age with uncertainty as low as 11% (Bellinger et al. 2019). However, it needs high-cadence photometric observations of stars spread over a long observation window, which is available only for a few hundred targets. Additionally, it only applies to stars hotter than about spectral type K because cooler stars generally do not show oscillations, which are necessary for determining the ages using asteroseismology (Silva Aguirre et al. 2015; Christensen-Dalsgaard & Aguirre 2018). The isochrone fitting approach, in which the ages are determined by positioning the star in the HR diagram, is another well-known and often employed technique. However, isochrone fitting can have large age uncertainties, typically up to 20% or more for the main-sequence stars (Tayar et al. 2022).

Nevertheless, to independently check the age trends in our sample, we used isochrone models from the Modules for Experiments in Stellar Astrophysics (MESA; Paxton et al. 2011, 2013, 2015, 2018) isochrones & Stellar Tracks (MIST; Choi et al. 2016; Dotter 2016) using the Python-based isoclassify[13] (Huber et al. 2017; Berger et al. 2020b). For the input parameters, we used GAIA spectroscopic parameters that are listed in the Astrophysical parameters table (calibrated as outlined in Appendix), together with parallaxes and *G*-band magnitudes taken from the Gaia DR3 data. Typical uncertainties in stellar atmospheric parameters T_{eff}, log *g* and [Fe/H] are assumed to be 100 K, 0.1 dex, and 0.1 dex, respectively. The H-R diagram for the stars whose ages are estimated in this paper is shown in Figure 7. After applying the cutoffs as described in Section 2, the distribution for the stellar ages for our sample is shown in Figure 8. We find that the median age of giant planet-hosting stars to be ∼3.17 Gyr and for the small planet hosts to be ∼4.07 Gyr (Table 2). We performed an AD test, which yielded a small *p*-value ($p = 1.22 \times 10^{-5}$),

[13] https://github.com/danxhuber/isoclassify

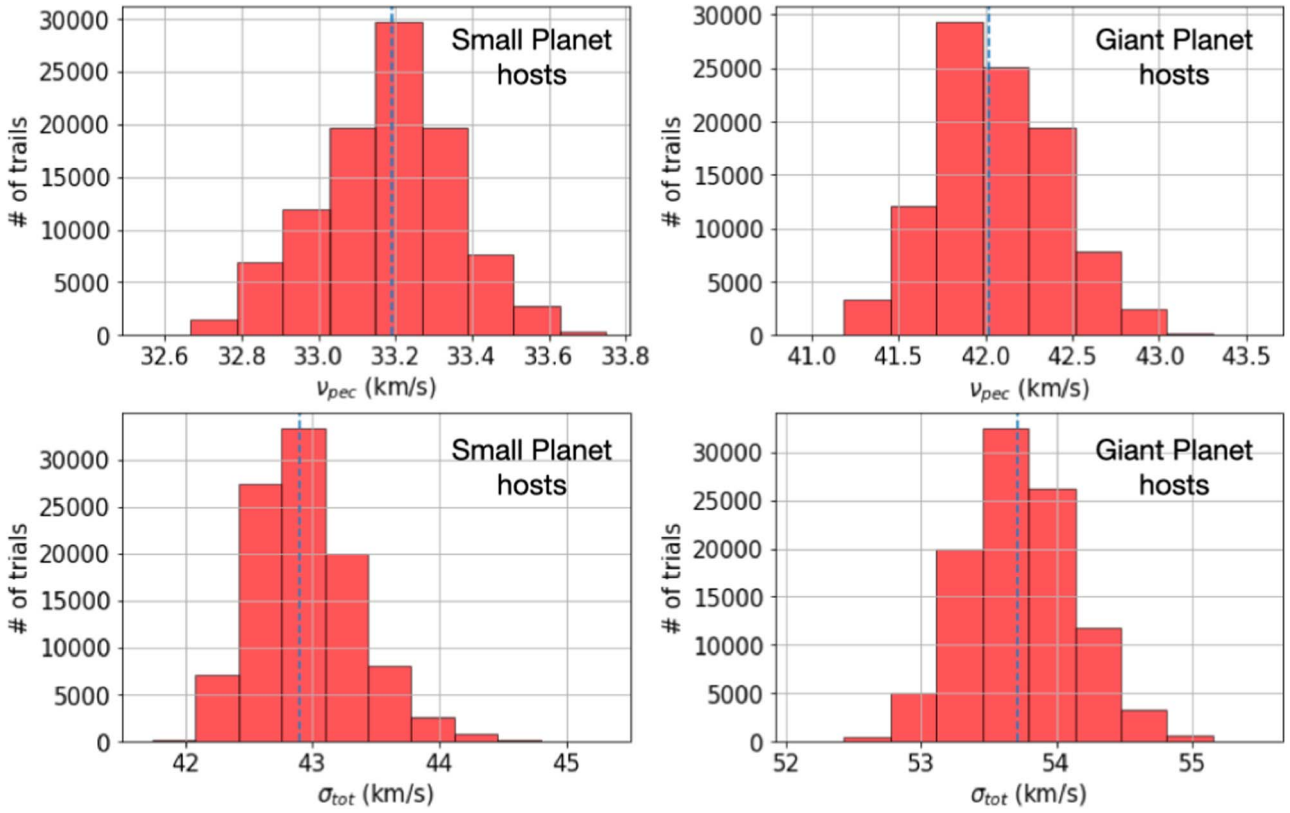

Figure 6. Distribution of ν_{pec} and σ_{tot} for the planet-hosting stars obtained from Monte Carlo simulation. The vertical-dashed lines represent the median of the distribution.

Table 2
Comparison of Small and Giant Planet-hosting Stars in Terms of Their Galactic Parameters and Ages Determined from the Isochrone Fitting

	Small planet	Giant planet	p-Value
Thin disk	1464	579	>0.05
Thick disk	29	7	>0.05
Z_{max} (kpc)	0.27 ± 0.12	0.21 ± 0.09	10^{-4}
Eccentricity	0.14 ± 0.07	0.11 ± 0.06	10^{-5}
ν_{pec} (km s^{-1})	42.79 ± 0.35	33.19 ± 0.18	10^{-6}
σ_{tot} (km s^{-1})	53.70 ± 0.41	42.89 ± 0.41	...
Ages (Gyr)	4.07 ± 3.23	3.17 ± 2.67	10^{-6}

Note. Errors represents the 1σ spread in the corresponding distribution of the parameters, except for ν_{pec} and σ_{tot}, where the 1σ spread is obtained from Monte Carlo method by taking into account for the uncertainties in U, V, and W (see text for more details). The p-value represents the probability of two samples belonging to the same distribution using the Anderson–Darling test.

indicating that the two data sets differ significantly in terms of their underlying distributions. However, given the large uncertainties in the individual age estimates using isochrone fitting, the AD test alone may not be a reliable predictor of the statistical significance of the age difference between the two distributions. To assess whether the population-level difference is statistically significant, we need to account for the individual age uncertainties associated with isochrone fitting. For that, we again performed a Monte Carlo experiment similar to the one described in Section 3.2. For each star, we randomly draw the age from the Gaussian distribution, whose mean and sigmas are estimated from the isochrone modeling. Repeating over the entire sample, the MC age distribution was obtained for stars with small and giant planet-hosting stars. We then compare

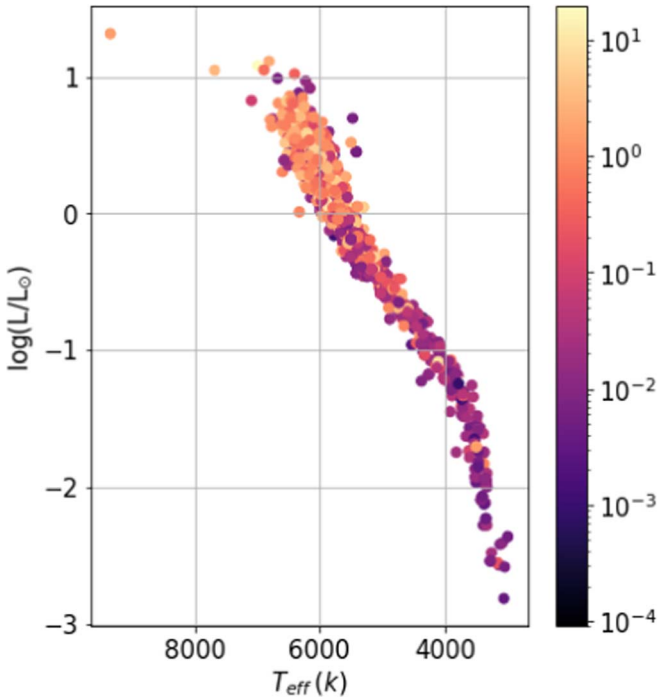

Figure 7. Hertzsprung–Russell Diagram for Stars with Determined Ages in this Study. The color bar on the left-hand side indicates the planet mass in units of M_j.

two populations to obtain the p-value using the AD test. Once the p-value is noted, we repeated the analysis 1,00,000 times. From the assemblage of p-values, we find that the p-value was smaller than 0.05 about 99% of the time, as shown in Figure 9.

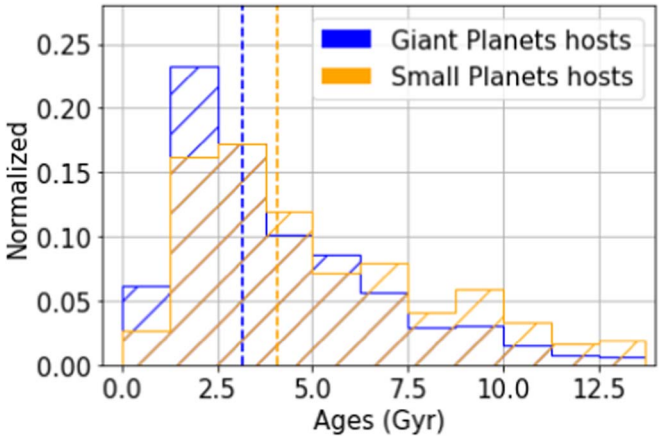

Figure 8. Age distribution for a sample of 807 planet-hosting stars from the MIST isochrone models (binned at 1.25 Gyr). The vertical lines represent the median age.

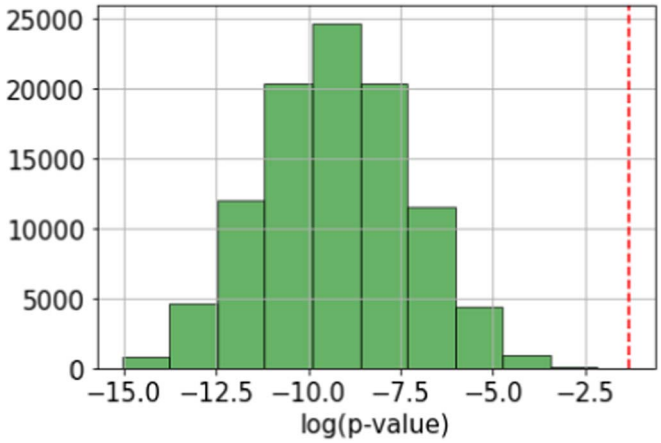

Figure 9. Distribution of p-values from the 1,00,000 AD test performed using Monte Carlo method. The black-dashed line represents the $p = 0.05$, below which two distributions are considered to be statistically different.

This numerical experiment clearly indicates that the population-level differences in isochrone ages shown in Figure 8 are statistically significant.

4. Discussions

Several galactic orbital ($\sigma_{\rm tot}$, eccentricity and $Z_{\rm max}$) and spectroscopic ([Fe/H] and [α/Fe]) parameters are proxies to stellar ages. To study different exoplanet populations and their formation timeline, we investigated the ages of their host stars. Our analysis shows that small planet-hosting stars have higher $\sigma_{\rm tot}$, eccentricity, $Z_{\rm max}$, and [α/Fe], and lower [Fe/H] when compared to stars hosting giant planets. Since higher $\sigma_{\rm tot}$, eccentricity, $Z_{\rm max}$, and [α/Fe] are indicators of an older population (Chen 2003; Casagrande et al. 2011; Wojno et al. 2018; Ness et al. 2019; Bashi & Zucker 2022), we find that the small planet-hosting stars are statistically older when compared to their giant planet hosts. To validate this, we used the isochrones fitting technique to estimate the stellar ages, using MIST isochrone grids, and we arrived at similar conclusions. While the majority of our planet-hosting stars primarily belong to the thin disk population and exhibit a predominance of higher metallicity (see Figure A1 of Swastik et al. 2022), we conducted additional investigations to determine to what extent the stars hosting small and giant planets are younger. This analysis involved controlling for the correlation between planet mass and stellar metallicity, considering that stellar ages are directly influenced by various stellar properties, including mass and radius. For instance, for a controlled stellar sample with the criteria of $-0.2 <$ [Fe/H] < 0.4 and $0.7R_{\rm Sun} < R_{\rm star} < 1.3R_{\rm Sun}$, we examined the extent to which the histogram offsets persisted. Notably, although the offsets were still observable, they exhibited a decrease and the histogram peaks shifted toward younger ages. This is expected because we selectively removed stars from specific age groups (older in this case) within the sample. We also repeated this analysis for other combinations and found similar trends. The fact that young metal-rich stars have a preference for hosting giant planets aligns with the natural progression of the chemical evolution of the galaxy and it is more challenging for giant planets to form around older metal-poor stars.

Radial velocity (RV) and transit detection are two of the most popular techniques used to detect exoplanets. However, these techniques have inherent biases that can impact our understanding of exoplanet populations (Swastik et al. 2022). For example, the radial velocity technique can detect massive planets that are close to their host star and have intermediate orbital periods (up to $\sim$10 au). However, stellar activity and line-broadening mechanisms reduce RV precision, and therefore very active and fast-rotating stars are usually excluded from the RV surveys. Meanwhile, the transit method is more sensitive to short orbital period planets (mostly below $\sim$1 au) whose orbits are favorably aligned along the observer's line of sight. Both of these methods have their own detection biases, and therefore lead to a non-representative sample of the true exoplanet population in the galaxy. For instance, younger stars have large variability,and consequently finding smaller planets around stars is more challenging (Vanderburg et al. 2016).

It is possible that some small planets might have missed detection around young stars due to sensitivity limitations. However, the different age proxies used in this work indicate that older stars have fewer giant planets compared to younger stars. The fact that giant planets are easier to detect irrespective of detection technique or the age of the star indicates that the overall occurrence rate of giant planets is much less around old stars (also shown from isochrone ages using the Kepler sample in Swastik et al. 2023, in preparation) and suggest that giant planets may have started forming late in the galaxy.

Stars and planets both originate from the same molecular cloud within the interstellar medium (ISM), and the metal content in the ISM is a crucial factor in the formation of planets. Our study reveals a significant finding that stars hosting giant planets are statistically associated with a younger population. For the formation of a giant planet, a core of $\sim$10 $M_{\oplus}$ must be formed within a relatively short timeframe of around 10 million years (Pollack et al. 1996) before the dissipation of gas in the protoplanetary disk. This core primarily consists of refractory elements, including both α-elements (e.g., Mg, Si, Ca, etc.) and Fe-peak elements (e.g., Fe, Ni, etc.). During the demise of the first stars as core-collapse supernovae (SNe II), the interstellar medium (ISM) became enriched with α-elements. However, during the early stages of the Milky Way's existence, the ISM lacked sufficient enrichment in heavy elements, particularly Fe-peak elements. This limitation hindered the core-accretion process necessary

for the formation of giant planets (Rice & Armitage 2003; Matsuo et al. 2007; Drazkowska et al. 2023). With the gradual enrichment of the ISM through Type Ia supernovae (SNe Ia), the availability of more Fe-peak elements (e.g., Fe, Ni, Cr, Mn, etc.) facilitated the onset of giant planet formation (Matteucci & Francois 1989; Alibés et al. 2001; Matteucci et al. 2009; Kobayashi et al. 2020; Swastik et al. 2022). Therefore, the scarcity of giant planets around older stars and the widely-observed planet-mass and stellar-metallicity correlation can be understood as a natural outcome of the galactic chemical evolution of the Milky Way. Seen that way, the temporal offset between the formation of small and giant planets will also be consistent with chemo-kinematic trends of planet-hosting stars and the mass–metallicity relationship.

5. Conclusions

The properties of exoplanets are closely related to the traits of their stellar hosts. In this work, we studied the chemical abundances, kinematics, and ages of planet-hosting stars. We used the GAIA DR3 data, for which the stellar parameters are available for the large number of exoplanet-hosting stars whose parameters have been estimated uniformly. We analyzed the astrometric, photometric, and spectroscopic data from the GAIA DR3. Here, we present a brief summary of our analysis:

1. Using the GAIA spectroscopic metallicities and abundances from the RVS spectra, we find that the host stars of giant planets are metal-rich and α-poor compared to small planet-hosting stars. This finding indicates that host stars of giant planets belong to a younger population of stars that started forming in the later stages of the galaxy after the enrichment of ISM with Fe-peak elements.
2. We find that most of our planet-hosting stars belong to the thin disk population, indicating that the overall sample of exoplanet-hosting stars belongs to the younger generations. For the galactic space velocities and orbital parameters, we find that host stars of small and Jupiter-like planets belong to a separate population. We also find that small planet-hosting stars have higher $Z_{\rm max}$ and eccentricities (which is a signature for older stars) when compared to giant planet-hosting stars.
3. By using the MIST isochrone models, we were able to estimate the approximate ages of the stars which host exoplanets. Our analysis reveals that stars which host giant planets are likely to be younger than those which host small planets, despite the fact that there are considerable uncertainties in the age estimates that are obtained from isochrones.

The present observations using the latest GAIA DR3 data suggest that the giant planets started forming at the later stages of the GCE evolution when the ISM was sufficiently enriched with Fe-peak elements by Type Ia supernovae, which happened around $\lesssim$6 Gyr. The enrichment of ISM is necessary to form the core of the giant planets faster before the dissipation timescale of the gas in the protoplanetary disk. Our results are also consistent with the core-accretion theory of planet formation (Pollack et al. 1996; Matsuo et al. 2007; Birnstiel et al. 2016; Owen & Murray-Clay 2018; Drazkowska et al. 2023). Future missions consisting of astrometry, photometry, and spectroscopic investigations should focus on a larger sample of exoplanet-hosting stars, measuring their chemical abundances and astrometric parameters uniformly and more precisely to support these findings.

Acknowledgments

This work has made use of data from (a) the NASA Exoplanet Archive, which is run by the California Institute of Technology under an Exoplanet Exploration Program contract with NASA, (b) the GAIA space mission by the European Space Agency (ESA; the data was processed by the Gaia Data Processing and Analysis Consortium (DPAC), and funding for the DPAC has been provided by national institutions, in particular, the institutions participating in the Gaia Multilateral Agreement), and (c) the exoplanet.eu database, which compiles and organizes data from various sources, including ground-based and space-based telescopes. We gratefully thank the anonymous referee for their insightful review and comments, which helped us improve this paper. Additionally, C.S. would like to thank Luca Casagrande, Partha Pratim Goswami and Sioree Ansar for numerous discussions on stellar kinematics.

Software: Numpy (Harris et al. 2020), Topcat (Taylor 2005), Astropy (Astropy Collaboration et al. 2013), Scikit-learn (Pedregosa et al. 2011), Matplotlib (Hunter 2007), Scipy (Virtanen et al. 2020).

Appendix
Calibration of Metallicities and Abundances

Although GAIA-DR3 provides the homogeneous estimation of stellar parameters for the largest number of stars to date, it requires several calibrations and filtering for any rigorous scientific study. For instance, the data from the GAIA-GSP spec module suffers from systematic (Recio-Blanco et al. 2023), and hence one needs to account for such biases to perform any meaningful analysis on the data. Although some calibrations have been already been proposed for GAIA data using three major ground-based surveys: APOGEE-DR17 (Abdurro'uf et al. 2022), RAVE-DR6 (Steinmetz et al. 2020), and GALAH-DR3 (Buder et al. 2021), we still find a significant offset and scatter in the calibrated data, as shown in Table 3 (last two rows), when compared to high-resolution and high SNR spectroscopic data from the HARPS-GTO sample (Mayor et al. 2003; Lo Curto et al. 2010; Santos et al. 2011). In addition, the calibration polynomials are established for stars with a wide range of atmospheric parameters in $\log g$ and $T_{\rm eff}$, and thus we decided to use our own tailored calibration for our sample of planet-hosting stars. Therefore, we use the HARPS-GTO sample (Mayor et al. 2003; Lo Curto et al. 2010; Santos et al. 2011), which is a survey of 1111 stars that were chosen to detect planets by radial velocity and also have a similar range of atmospheric parameters as that of the planet-hosting stars used in this paper. Although the wavelength coverage of HARPS (378–691 nm) and GAIA (846–870 nm) is different, it will not affect the estimate of stellar atmospheric parameters because there are sufficient Fe-lines to estimate the metallicities. We cross-matched our sample and found 932 common stars between the HARPS and the GAIA samples. Upon comparing the metallicities of the stars from GAIA and HARPS, as shown in Figure 10, we find that the distribution about the $x = y$ line is not symmetric. In addition, we also find a temperature gradient with [Fe/H], where the [Fe/H] is underestimated for hotter stars ($\geqslant$ 5500 K) and overestimated for cooler stars ($\leqslant$5500 K). Therefore, to account for the temperature dependence, we analyzed the δ[Fe/H] = [Fe/H]$_{\rm GAIA}$-[Fe/H]$_{\rm HARPS}$ as a function of $T_{\rm eff}$. The relationship between the δ[Fe/H] and $T_{\rm eff}$ can be best described by a

Table 3
Differences in Median Offset and Robust Sigma between GAIA GSP-Spec and Individual Surveys

	$T_{\rm eff}$	log(g)	(M/H)	log(g)$_{\rm calibration}$	(M/H)$_{\rm calibration}$
RAVE-DR6	(−12; 93)	(−0.28; 0.19)	(−0.05; 0.11)	(−0.003; 0.18)	(−0.05; 0.09)
APOGEE-DR17	(−32; 86)	(−0.32; 0.17)	(0.04; 0.12)	(−0.005; 0.15)	(0.06; 0.12)
GALAH-DR3	(20; 87)	(−0.26; 0.21)	(0.01; 0.10)	(0.003; 0.18)	(−0.001; 0.10)
HARPS-GTO (current work using Equation (A1)))	(−12, 97)	(−0.24, 0.30)	(−0.04, 0.08)	(−0.05, 0.25)	(0.001, 0.07)
HARPS-GTO (with GAIA proposed polynomial)				(−0.18, 0.24)	(−0.07, 0.09)

Note. The first three rows are taken from Table D1 of Recio-Blanco et al. (2023). The values in the parenthesis are median offset, followed by robust sigma (standard deviation obtained by removing outliers) computed from the residuals. The last two rows are for HARPS-GTO data with the calibration results from Equation (A1), and GAIA proposed polynomials.

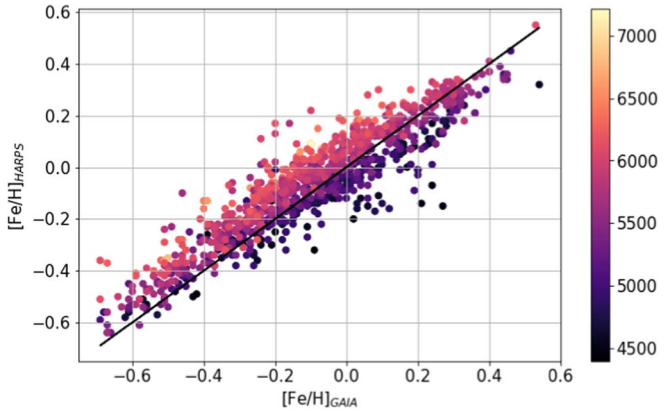

Figure 10. Comparison of the [Fe/H] values from GAIA GSP-Spec module and the HARPS sample. The black line is the $x = y$ line and the color bar on the right-hand side represents the effective temperature of the star.

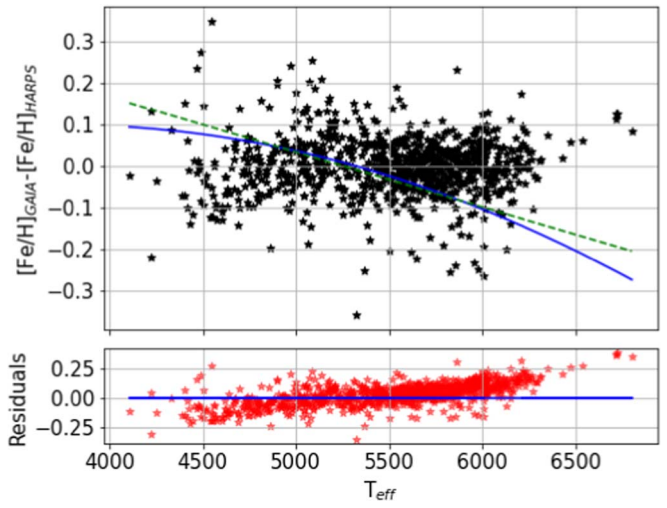

Figure 11. Comparison of δ[Fe/H] = [Fe/H]$_{\rm GAIA}$-[Fe/H]$_{\rm HARPS}$ as a function of $T_{\rm eff}$. A quadratic polynomial best describes the trends of δ[Fe/H] with $T_{\rm eff}$. The blue line is the best-fit polynomial with the coefficients (p0, p1, p2) = (−3.96e–08, 2.97e–04, −4.57e–01) for the top figure, while the bottom figure shows the residuals in the approximation of the trend by the above polynomial. The green-dashed line shows the linear fit for the data.

quadratic polynomial (Figure 11), as given below:

$$\delta[{\rm Fe/H}] = [{\rm Fe/H}]_{\rm GAIA} - [{\rm Fe/H}]_{\rm HARPS} = \sum_{i=0}^{2} p_i . T_{\rm eff}^{i} \quad \text{(A1)}$$

Thus, for a given $T_{\rm eff}$, we compute the δ[Fe/H] using Equation (A1) to estimate the offset in [Fe/H]. We then calibrated our data using Equation (A1) and checked for any remaining offset in the HARPS-GTO and GAIA calibrated data using our calibrations. We find no significant offset between GAIA calibrated and HARPS-GTO data as listed in Table 3. We then applied the same correction to the sample of planet-hosting stars to correct the estimation bias and then used those calibration values to study the correlation trends.

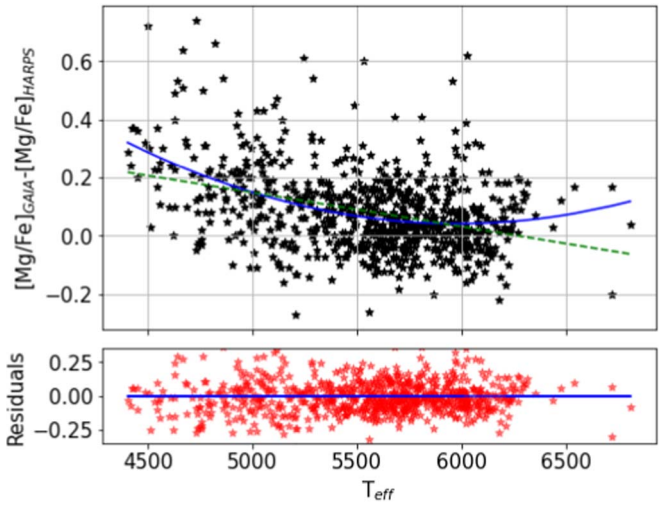

Figure 12. Variation of δ[Mg/Fe] = [Mg/Fe]$_{\rm GAIA}$-[Mg/Fe]$_{\rm HARPS}$ as a function of effective temperature. A quadratic polynomial best describes the trends of δ[Mg/Fe] with $T_{\rm eff}$. The best-fit polynomial is represented by the blue line in the top figure, by the coefficients (p0, p1, p2) = (1.12e–07, -1.34e–03, 4.05), while the figure at the bottom shows the residuals in the approximation of the trend by the above polynomial. The green-dashed line shows the linear fit for the data.

We performed a similar calibration for alpha-elements and found a temperature gradient with a difference of α-abundances. Since Mg is the strongest tracer for α abundances (Kobayashi et al. 2020; Swastik et al. 2022), we analyze the [Mg/Fe] from the HARPS and the GAIA sample. Figure 12 shows the δ[Mg/Fe] as a function of $T_{\rm eff}$. We used the calibration procedure, similar to [Fe/H], and then applied the suitable corrections for the planet-hosting stars.

ORCID iDs

C. Swastik https://orcid.org/0000-0003-1371-8890
Ravinder K. Banyal https://orcid.org/0000-0003-0799-969X
Mayank Narang https://orcid.org/0000-0002-0554-1151
Athira Unni https://orcid.org/0000-0001-6093-5455
Bihan Banerjee https://orcid.org/0000-0001-8075-3819

P. Manoj https://orcid.org/0000-0002-3530-304X
T. Sivarani https://orcid.org/0000-0003-0891-8994

References

Abdurro'uf, Accetta, K., Aerts, C., et al. 2022, ApJS, 259, 35
Adibekyan, V. Z., Santos, N. C., Sousa, S. G., et al. 2012, A&A, 543, A89
Adibekyan, V. Z., Santos, N. C., Sousa, S. G., & Israelian, G. 2011, A&A, 535, L11
Akeson, R. L., Chen, X., Ciardi, D., et al. 2013, PASP, 125, 989
Alibés, A., Labay, J., & Canal, R. 2001, A&A, 370, 1103
Armstrong, D. J., Meru, F., Bayliss, D., Kennedy, G. M., & Veras, D. 2019, ApJL, 880, L1
Astropy Collaboration, Robitaille, T. P., Tollerud, E. J., et al. 2013, A&A, 558, A33
Bashi, D., & Zucker, S. 2022, MNRAS, 510, 3449
Bellinger, E. P., Hekker, S., Angelou, G. C., Stokholm, A., & Basu, S. 2019, A&A, 622, A130
Berger, T. A., Huber, D., Gaidos, E., & van Saders, J. L. 2018, ApJ, 866, 99
Berger, T. A., Huber, D., Gaidos, E., van Saders, J. L., & Weiss, L. M. 2020a, AJ, 160, 108
Berger, T. A., Huber, D., van Saders, J. L., et al. 2020b, AJ, 159, 280
Birnstiel, T., Fang, M., & Johansen, A. 2016, SSRv, 205, 41
Bonfanti, A., Ortolani, S., Piotto, G., & Nascimbeni, V. 2015, A&A, 575, A18
Bovy, J. 2015, ApJS, 216, 29
Brewer, J. M., & Fischer, D. A. 2018, ApJS, 237, 38
Brewer, J. M., Fischer, D. A., Valenti, J. A., & Piskunov, N. 2016, ApJS, 225, 32
Buchhave, L. A., Bizzarro, M., Latham, D. W., et al. 2014, Natur, 509, 593
Buchhave, L. A., Latham, D. W., Johansen, A., et al. 2012, Natur, 486, 375
Buder, S., Sharma, S., Kos, J., et al. 2021, MNRAS, 506, 150
Casagrande, L., Schönrich, R., Asplund, M., et al. 2011, A&A, 530, A138
Chen, C. 2003, ScChA, 46, 1
Chen, J., & Kipping, D. 2017, ApJ, 834, 17
Choi, J., Dotter, A., Conroy, C., et al. 2016, ApJ, 823, 102
Christensen-Dalsgaard, J., & Aguirre, V. S. 2018, in Handbook of Exoplanets, ed. H. J. Deeg & J. A. Belmonte (New York: Springer), 184
Cropper, M., Katz, D., Sartoretti, P., et al. 2018, A&A, 616, A5
Delgado Mena, E., Moya, A., Adibekyan, V., et al. 2019, A&A, 624, A78
Dong, S., Zheng, Z., Zhu, Z., et al. 2014, ApJL, 789, L3
Dotter, A. 2016, ApJS, 222, 8
Drazkowska, J., Bitsch, B., Lambrechts, M., et al. 2023, in ASP Conf. Ser. 534, Protostars and Planets VII, ed. S. Inutsuka et al. (San Francisco, CA: ASP), 717
Fischer, D. A., & Valenti, J. 2005, ApJ, 622, 1102
Fleming, S. W., Mahadevan, S., Deshpande, R., et al. 2015, AJ, 149, 143
Fulton, B. J., Petigura, E. A., Howard, A. W., et al. 2017, AJ, 154, 109
Gonzalez, G. 1997, MNRAS, 285, 403
Gaia Collaboration, Brown, A. G. A., Vallenari, A., et al. 2018, A&A, 616, A1
Gaia Collaboration, Vallenari, A., Brown, A. G. A., et al. 2022, arXiv:2208.00211
Harris, C. R., Millman, K. J., van der Walt, S. J., et al. 2020, Natur, 585, 357
Huber, D., Zinn, J., Bojsen-Hansen, M., et al. 2017, ApJ, 844, 102
Hunter, J. D. 2007, CSE, 9, 90
Johnson, D. R. H., & Soderblom, D. R. 1987, AJ, 93, 864
Johnson, J. A., Petigura, E. A., Fulton, B. J., et al. 2017, AJ, 154, 108
Kobayashi, C., Karakas, A. I., & Lugaro, M. 2020, ApJ, 900, 179
Lo Curto, G., Mayor, M., Benz, W., et al. 2010, A&A, 512, A48
Matsuo, T., Shibai, H., Ootsubo, T., & Tamura, M. 2007, ApJ, 662, 1282
Matteucci, F., & Francois, P. 1989, MNRAS, 239, 885
Matteucci, F., Spitoni, E., Recchi, S., & Valiante, R. 2009, A&A, 501, 531
Mayor, M., Pepe, F., Queloz, D., et al. 2003, Msngr, 114, 20
Mulders, G. D. 2018, Planet Populations as a Function of Stellar Properties, 153
Narang, M., Manoj, P., Furlan, E., et al. 2018, AJ, 156, 221
NASA Exoplanet Science Institute 2020, Planetary Systems Table, IPAC
Ness, M. K., Johnston, K. V., Blancato, K., et al. 2019, ApJ, 883, 177
Owen, J. E., & Murray-Clay, R. 2018, MNRAS, 480, 2206
Paxton, B., Bildsten, L., Dotter, A., et al. 2011, ApJS, 192, 3
Paxton, B., Cantiello, M., Arras, P., et al. 2013, ApJS, 208, 4
Paxton, B., Marchant, P., Schwab, J., et al. 2015, ApJS, 220, 15
Paxton, B., Schwab, J., Bauer, E. B., et al. 2018, ApJS, 234, 34
Pedregosa, F., Varoquaux, G., Gramfort, A., et al. 2011, JMLR, 12, 2825
Perryman, M., Hartman, J., Bakos, G. Á., & Lindegren, L. 2014, ApJ, 797, 14
Petigura, E. A., Marcy, G. W., Winn, J. N., et al. 2018, AJ, 155, 89
Petigura, E. A., Rogers, J. G., Isaacson, H., et al. 2022, AJ, 163, 179
Pollack, J. B., Hubickyj, O., Bodenheimer, P., et al. 1996, Icar, 124, 62
Pont, F., & Eyer, L. 2004, MNRAS, 351, 487
Recio-Blanco, A., de Laverny, P., Allende Prieto, C., et al. 2016, A&A, 585, A93
Recio-Blanco, A., de Laverny, P., Palicio, P. A., et al. 2023, A&A, 674, A29
Reddy, B. E., Lambert, D. L., & Allende Prieto, C. 2006, MNRAS, 367, 1329
Rice, W. K. M., & Armitage, P. J. 2003, ApJL, 598, L55
Santos, N. C., Israelian, G., & Mayor, M. 2001, A&A, 373, 1019
Santos, N. C., Mayor, M., Bonfils, X., et al. 2011, A&A, 526, A112
Schlaufman, K. C. 2018, ApJ, 853, 37
Schönrich, R., Binney, J., & Dehnen, W. 2010, MNRAS, 403, 1829
Silva Aguirre, V., Davies, G. R., Basu, S., et al. 2015, MNRAS, 452, 2127
Steinmetz, M., Matijevič, G., Enke, H., et al. 2020, AJ, 160, 82
Swastik, C., Banyal, R. K., Narang, M., et al. 2021, AJ, 161, 114
Swastik, C., Banyal, R. K., Narang, M., et al. 2022, AJ, 164, 60
Tayar, J., Claytor, Z. R., Huber, D., & van Saders, J. 2022, ApJ, 927, 31
Taylor, M. B. 2005, in ASP Conf. Ser. 347, Astronomical Data Analysis Software and Systems XIV, ed. P. Shopbell, M. Britton, & R. Ebert (San Francisco, CA: ASP), 29
Udry, S., & Santos, N. C. 2007, ARA&A, 45, 397
Ujjwal, K., Kartha, S. S., Mathew, B., Manoj, P., & Narang, M. 2020, AJ, 159, 166
Unni, A., Narang, M., Sivarani, T., et al. 2022, AJ, 164, 181
Valenti, J., & Fischer, D. 2008, in ASP Conf. Ser. 384, 14th Cambridge Workshop on Cool Stars, Stellar Systems, and the Sun, ed. G. van Belle (San Francisco, CA: ASP), 292
van Leeuwen, F. 1997, SSRv, 81, 201
Vanderburg, A., Plavchan, P., Johnson, J. A., et al. 2016, MNRAS, 459, 3565
Virtanen, P., Gommers, R., Oliphant, T. E., et al. 2020, NatMe, 17, 261
Wojno, J., Kordopatis, G., Steinmetz, M., et al. 2018, MNRAS, 477, 5612
Zhao, H., Schultheis, M., Rojas-Arriagada, A., et al. 2021, A&A, 654, A116